Journal of Materials Science & Technology 101 (2022) 107–117

Contents lists available at ScienceDirect

Journal of Materials Science & Technology

journal homepage: www.elsevier.com/locate/jmst

Research Article

Surface decoration of Halloysite nanotubes with POSS for fire-safe thermoplastic polyurethane nanocomposites

Wei Wu[a,b], Wanjing Zhao[b], Xianjing Gong[a], Qijun Sun[a], Xianwu Cao[b], Yujun Su[c], Bin Yu[d,*], Robert K.Y. Li[a], Roy A.L. Vellaisamy[e,*]

[a] Department of Materials Science and Engineering, City University of Hong Kong, Tat Chee Avenue, Kowloon, Hong Kong SAR, China
[b] National Engineering Research Center of Novel Equipment for Polymer Processing, Key Laboratory of Polymer Processing Engineering of Ministry of Education, Guangdong Provincial Key Laboratory of Technique and Equipment for Macromolecular Advanced Manufacturing, School of Mechanical and Automotive Engineering, South China University of Technology, Guangzhou 510640, China
[c] National-certified Enterprise Technology Center, Kingfa Science and Technology Co. Ltd., Guangzhou 510663, China
[d] Centre for Future Materials, University of Southern Queensland, Toowoomba, Queensland, Australia
[e] James Watt School of Engineering, University of Glasgow, Glasgow G12 8QQ, United Kingdom

ARTICLE INFO

Article history:
Received 28 March 2021
Revised 1 May 2021
Accepted 7 May 2021
Available online 5 August 2021

Keywords:
Thermoplastic polyurethane
Halloysite nanotube
POSS
Flame retardancy
Mechanical property

ABSTRACT

Halloysite nanotubes (HNTs) have been considered as a promising flame retardant fillers for polymers. In this work, the polyhedral oligomericsilsesquioxane (POSS) containing amino group was covalently grafted on the surface of HNTs with 3-(2,3-epoxypropoxy)propytrimethoxysilane as a chemical bridge. The POSS modified HNTs (HNTs-POSS) dispersed uniformly in the thermoplastic polyurethane (TPU) matrix and endowed TPU nanocomposites with enhanced tensile properties and fire safety. Cone calorimeter tests revealed that the introduction of 2 wt% HNTs-POSS to TPU matrix remarkably reduced the peak of heat release rate (PHRR) and total heat release (THR) by 60.0% and 18.3%, respectively. In addition, the peak CO production rate and total smoke release (TSR) could be significantly suppressed by the addition of HNTs-POSS. The well dispersed HNTs in combination with the ceramified silicon network from the thermal decomposition of POSS contributed to the formation of a continuous and compact char layer, exhibiting a tortuous effect by inhibiting heat diffusion and evaporation of volatile gaseous. In addition, the released crystal water from HNTs could dilute the combustible volatiles and then decline the combustion intensity. The tensile tests demonstrated that introduction of 2 wt% HNTs-POSS would enhance the maximum stress of TPU nanocomposite with a slight decrease of elongation at break. The combination of HNTs and POSS through the construction of effective interfacial interactions provides a feasible way to effectively enhance the fire safety of TPU nanocomposites without scarifying ductility.

1. Introduction

Thermoplastic polyurethane (TPU) has received considerable attention to exploit its applications in various fields, such as automobile, aerospace and building, due to its superior mechanical properties, adjustable flexibility, and good chemical resistance [1–4]. However, the intrinsic high flammability and the release of toxic fumes of TPU during combustion pose a big potential threat to people's lives and property, which restrict its broad applications. To improve the fire safety of TPU, various nanomaterials have been utilized as flame retardant additives to incorporate into the TPU matrix. With the incorporation of 2 wt% of MXene and rGO hybrids, the total smoke release (TSR) and peak of smoke production rate (pHRR) of TPU nanocomposite were dramatically reduced by 54.0% and 81.2%, respectively, as compared with that of pure TPU [5]. Shi et al. [6] found graphitic carbon nitride in combination of spinel copper cobaltate suppressed the pyrolysis gaseous of TPU significantly. The pHRR and THR of TPU composites decreased by 37% and 31.3%, respectively. Ji et al. [7] demonstrated that TPU ternary composites containing 1 wt% CNT and 10 wt% intumescent flame retardants (IFRs) exhibited good flame retardancy with high electromagnetic interference shielding efficiency. The introduction of CNTs contributed to enhancing the carbonization effect of IFRs. Graphene was mixed with different flame retardant additives to improve the thermal stability and fire safety of TPU [8,9]. The results revealed that the well dispersed graphene could hin-

* Corresponding authors.
E-mail addresses: ahu07yb@gmail.com (B. Yu), roy.vellaisamy@glasgow.ac.uk (R.A.L. Vellaisamy).

https://doi.org/10.1016/j.jmst.2021.05.060
1005-0302/

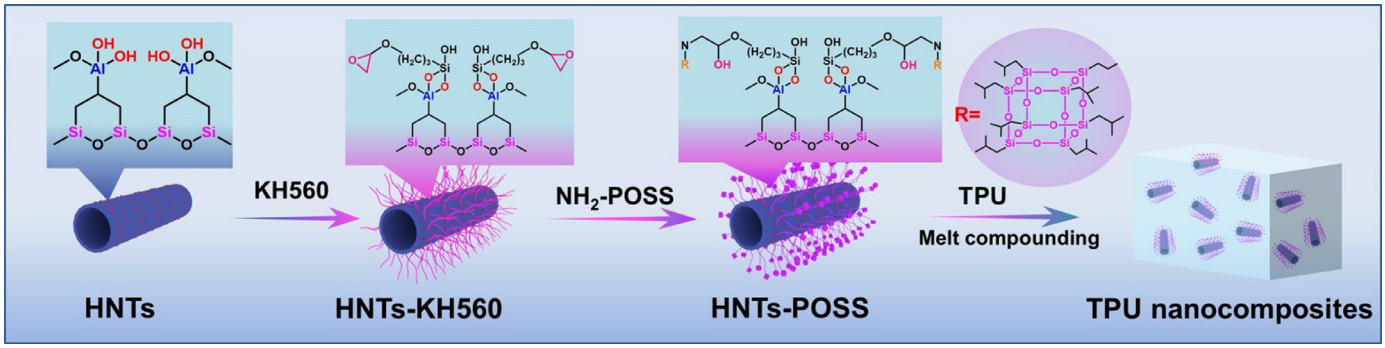

Scheme 1. Preparation route of TPU/HNTs-POSS nanocomposites.

der the escape of volatile gaseous with barrier function. Yu et al. [10] exhibited that the addition of layered MXene nanosheets contributed to forming thermally insulating char layer and catalyzing the generation of TiO_2 during the combustion of TPU. In order to satisfy the continuous increasing requirement of fire safety, it is important to explore new functional nanofillers.

Polyhedral oligomericsilsesquioxane (POSS) is a type of inorganic/organic hybrid material, which consists of an inorganic Si-O-Si core surrounded by different organic groups [11,12]. Because it combines the advantages of inorganic materials with those of organic polymers, it is considered as a new generation of multifunctional filler. Over the years, POSS has been used as a promising additive for flame retarded and/or reinforced TPU. Bourbigot et al. [13] found that the pHRR of TPU/POSS composites containing 10 wt% POSS decreased by 80% as compared to pure TPU. This was due to the fact that POSS decomposition could form a ceramic-like silicon char network with a polyaromatic structure. Spoljaric and his colleagues [14] found the presence of POSS-Boltorn hybrids in TPU contributed to improving the thermal stability, tensile modulus and strength due to the enhanced interaction and restriction on TPU chain segments. The corner functional groups make POSS an ideal building block in combination with other fillers for high performance of TPU composites.

Halloysite nanotube (HNTs) is a type of natural tubular clay with a molecular formula $[Al_2Si_2O_5(OH)_4{\cdot}nH_2O)]$ [15]. It has been utilized as a multifunctional filler for polymer reinforcement [16,17], drug delivery [18], and water purification [19] due to its natural availability, high aspect ratio, hollow structure, and high density of hydroxyl groups on the surface. Recent research has demonstrated that HNTs can serve as a thermal insulation barrier to extend the ignition time, reduce the pHRR and improve the char residue of polymer during combustion [20–22]. Moreover, the tube shape of HNTs contributes to trapping the flammable volatiles [23]. Thus, HNTs are regarded as promising reinforcing and flame retardant nano-fillers for polymers. It is an effective way to modify the surface of HNTs to improve their flame retardant efficiency. Sahnouce et al. [24] modified HNTs with methyl phosphonic acid to enhance the fire safety of polyamide-11. Melamine was self-assembly coated on the surface of HNTs to reduce smoke release and fire hazard of polypropylene [25]. Wang et al. [26] mixed HNTs with soy proteins and ammonium polyphosphate as IFRs for poly (butylene succinate). Wang et al. [27] found the presence of silicone modified HNTs could twist with degraded polyporpylene chains to form “fiber-like” thick and dense char layers during combustion. Jin et al. [28] demonstrated that HNT immobilized by chitosan/tannic acid (CS/TA) complex could serve as a green flame retardant for PLA/bamboo fiber composites due to HNT contributed to form a continuous compact char layer. However, the application of HNTs in combination with POSS to enhance the fire safety of polymer composites has not been reported.

In this work, the POSS containing amino group was covalently grafted onto the surface of HNTs (HNTs-POSS) by using 3-(2,3-epoxypropoxy)propytrimethoxysilane as a chemical bridge. Then pristine HNTs and HNTs-POSS were incorporated into TPU by melt compounding, respectively. The comparison between the effects of the pristine HNTs and HNTs-POSS on the fire safety and mechanical properties of TPU was investigated. The limited oxygen index (LOI) and cone calorimeter were conducted to evaluate the flammability and fire safety of the prepared TPU nanocomposites, while tensile tests were utilized to investigate the mechanical properties. Moreover, the flame retardant mechanism of TPU nanocomposites was further analyzed.

2. Experimental

2.1. Materials

Thermoplastic polyurethane (TPU, Desmopan® 9385A) was supplied by Covestro (Shanghai, China). Halloysite nanotube (HNTs) was obtained from Yuan Xin Nano Technology Co. Ltd, (Guangzhou, China). Aminopropyl-isobutyl POSS (AM0265) was supplied by Hybrid Plastics (USA). The methanol, Tetrahydrofuran (THF) and 3-(2,3-epoxypropoxy)propytrimethoxysilane (KH-560) were purchased from J and K Chemical (Shanghai, China). All the chemicals and solvents were used without further purification.

2.2. Preparation of TPU composites

The POSS modified HNTs (HNTs-POSS) were synthesized by two steps, as shown in Scheme 1. Typically, 2.0 g HNTs was dispersed in 200 mL methanol with ultrasonication for 15 min. Subsequently, 300 μl 3-(2,3-epoxypropoxy)propytrimethoxysilane (KH560) was added dropwise into methanol. The mixture was stirred and refluxed at 75 °C for 4 h. The resultant solution was centrifuged (10,000 rpm, 10 min) and rinsed in methanol and DI water, respectively. The obtained HNTs-KH560 was dried in an air circulating drying oven. Then the 1.0 g as-prepared HNTs-KH560 with 0.5 g POSS were mixed in100 mL THF with vigorous stirring. The mixture was kept stirring and refluxed at 70 °C for 4 h. The obtained HNTs-POSS was centrifuged (10,000 rpm, 10 min) and washed with THF and DI water, respectively. The resultant powder was dried under vacuum for 12 h and used without further purification.

Prior to the nanocomposite preparation, TPU pellets were dried at 75 °C for 4 h to remove the absorbed water. Then TPU was mixed with the required amount of HNTs-POSS by melt-compounding (Brabender Mixer, 200 °C, 60 rpm, 8 min). The TPU/HNTs-POSS nanocomposites were abbreviated as HNTs-POSS-X, where X stands for the weight fraction of HNTs-POSS in the TPU nanocomposites. Afterwards, the TPU nanocomposites were hot-compressed at 190 °C for 10 min. For comparison, pristine HNTs

Table 1
The formulations of TPU nanocomposites.

Sample	TPU (wt%)	Pristine HNTs (wt%)	HNTs-POSS (wt%)
TPU	100	–	–
HNTs-0.5	99.5	0.5	–
HNTs-2	98	2	–
HNTs-POSS-0.5	99.5	–	0.5
HNTs-POSS-2	98	–	2

were incorporated into TPU in the same processing conditions. The formulations of TPU nanocomposites are shown in Table 1.

2.3. Characterization

The morphology and element analysis of the HNTs-POSS were recorded by a transmission electron microscope (JEOL JEM-2100F) equipped with an Oxford energy-dispersive X-ray (EDX) spectroscopy. The cross-sectional surfaces of the TPU composites samples were observed by FE-SEM (FEI Quanta FEG250) at 10 kV to observe the dispersion of the HNTs and HNTs-POSS in the TPU matrix. The samples were cryo-fractured in liquid nitrogen and sputter with gold before observation. The Fourier transform infrared spectroscopy (FT-IR) spectra were performed on a Nicolet NEXUS670 spectrometer in the wavenumber range of 400–4000 cm^{-1}. Each spectrum was recorded with 16 scans at a resolution of 1 cm^{-1}. X-ray photoelectron spectroscopy (XPS, Physical Electronics PHI-5802) equipped with a monochromatic AlK_α X-ray source (1486.6 eV) was utilized to characterize the elemental chemical states of pristine HNTs and HNTs-POSS. X-ray diffraction (XRD) patterns were carried out by an X-ray diffractometer (Bruker AXS D2) with CuK_α radiation. The data were collected in the 2θ range from 5° to 60° with a step of 0.02° (2θ). The thermal stability of the composites was evaluated by a thermogravimetric analyzer (TGA) (TG209F3, Netzch). Approximately 10 mg of the sample was heated from room temperature to 700 °C at a heating rate of 10 °C min^{-1} under air atmosphere. Limiting oxygen index (LOI) testing was performed on an oxygen index instrument (HC-2, Jiangning Analytical Instrument, China). The dimensions of the specimens were 100 × 6.5 × 3 mm^3. The flame-retardant tests were performed on a cone calorimeter instrument (Fire Testing Technology, UK) according to the standard of ISO 5660. The dimension of specimens was 100 × 100 × 3 mm^3. All test specimens were wrapped in aluminum foil and measured under an external heat flux of 35 kW m^{-2}. The Raman spectra of the char residues were collected from a con-focal microRaman system (LabRAM Aramis) equipped with a 532 nm internal laser. Thermogravimetric analysis-infrared spectrometry (TGA-IR, TA Q5000) was performed to analyze the volatilized products after the pyrolysis of the sample from 50 to 800 °C with a heating rate of 20 °C min^{-1} in nitrogen atmosphere. The tensile properties of the TPU composites were examined using an universal testing machine (Instron 5566) with a load cell of 10 kN. The dumbbell-shaped specimens with dimension of 75 × 5 × 1 mm^3 were tested at a tensile speed of 200 mm min^{-1}. The reported results were average values for at least five separate specimens.

3. Results and discussion

3.1. Characterization of HNTs-POSS

The morphology of pristine HNTs and HNTs-POSS is shown in Fig. 1. In Fig. 1(a, b), it is observed that the pristine HNTs and HNTs-POSS exhibit a typical tubular structure with an outer diameter of 90 nm, an inner diameter of 20 nm, and a length of about 700–1200 nm. Fig. 1(c) shows the STEM image of HNTs-POSS, and the corresponding EDX mapping images (Fig. 1(d–f)) confirm the presence of nitrogen, aluminum and silicon elements, respectively, indicating the POSS has been grafted on the surface of HNTs successfully.

To investigate the effect of grafted POSS on the bonds of HNTs-POSS, Fig. 2(a) depicts the FT-IR spectra of pristine HNTs and HNTs-POSS. The stretching vibration of hydroxyl groups in HNTs is responsible for the distant and strong peak at 3700 and 3200 cm^{-1} [29]. Two new peaks (3695 and 3622 cm^{-1}) in the HNTs-POSS curve are corresponding to the inner hydroxyl groups of HNTs, indicating the silane agent (KH-560) has reacted with the outer hydroxyl groups [20]. The characteristic peak at 1082 cm^{-1} is ascribed to the asymmetric stretching of Si-O-Si bands. The peak intensity of Si-O-Si bands in HNTs-POSS increases significantly as compared with that of pristine HNTs, which is due to the pres-

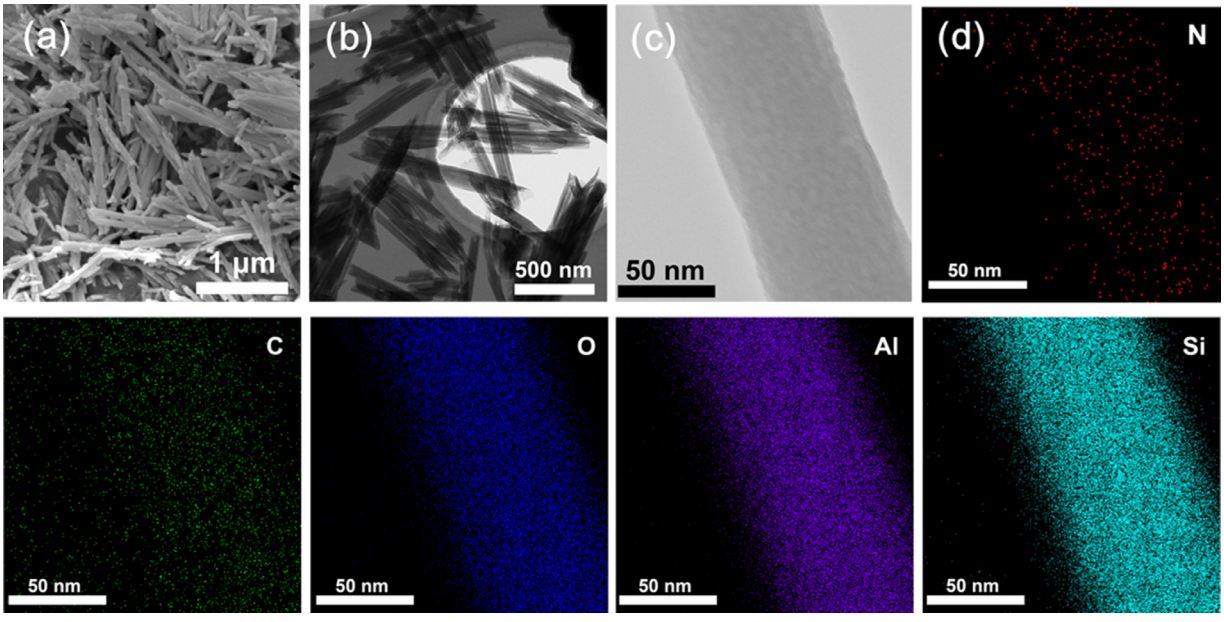

Fig. 1. (a) SEM image of pristine HNTs, (b) TEM image, (c) STEM image, and (d) EDX elemental mapping of N, C, O, Al, and Si of HNTs-POSS.

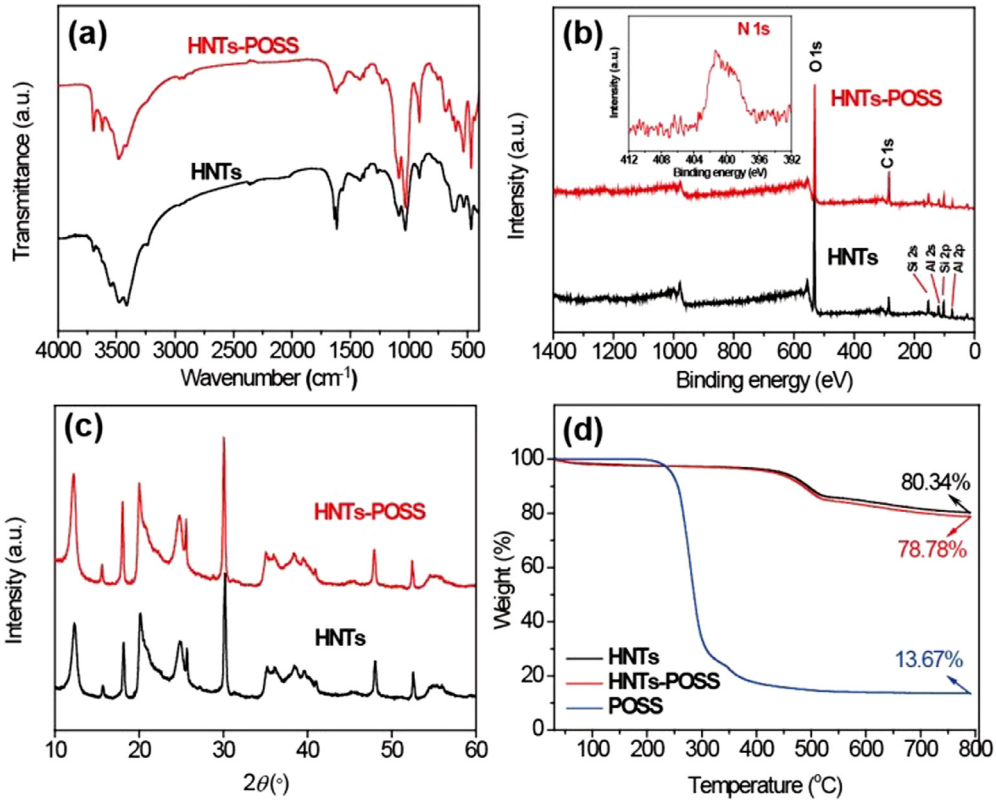

Fig. 2. (a) FT-IR spectra, (b) XPS survey spectrum, insert is high resolution spectrum of N 1s of HNTs-POSS (c) XRD patterns, and (d) TGA curves of pristine HNTs and HNTs-POSS.

ence of POSS. Moreover, two weak peaks appear in the range of 2950–2850 cm^{-1}, which are ascribed to the stretching vibration of isobutyl C-H bonds. Besides, the signal at 1218 cm^{-1} is assigned to the stretching vibration of the C-O-C band, which is derived from the grafted silane agent KH-560. From the FT-IR results, it clearly demonstrates the existence of POSS in HNTs-POSS. An X-ray photoelectron spectrum (XPS) scan of the HNTs-POSS is performed to further confirm the successful introduction of POSS on HNTs surface. The presence of oxygen (O 1s), silicon (Si 2s and Si 2p), and aluminum (Al 2s and Al 2p) in the spectrum in Fig. 2(b) is consistent with the composition of HNTs (Scheme 1). Moreover, the intensity of C 1s signal observed at 284.8 eV increased significantly resulting from the introduced silane agent. The high-resolution N 1s spectrum of HNTs-POSS also confirms the existence of nitrogen, which originates from the aminopropyl group in POSS. All the above results demonstrated the POSS has been successfully decorated on the surface of HNTs. The XRD patterns of pristine HNTs and HNTs-POSS show the same characteristic peaks in Fig. 2(c), suggesting the incorporation of POSS did not affect the crystal structure. The thermal stability of pristine HNTs and HNTs-POSS were investigated by TGA, as shown in Fig. 2(d). The weight loss between 30 and 150 °C is due to the release of absorbed water from the surface and internal channels of HNTs. The main weight loss stage in the range of 350–550 °C is attributed to the loss of inner water. As for the HNTs-POSS, it shows a slight decrease in the temperature of 200–350 °C, which is corresponding to the pyrolysis of grafted POSS. In addition, the char yields of pristine HNTs and HNTs-POSS at 800 °C are 80.34 wt% and 78.78 wt%, respectively. These results indicate that 11.41 wt% of POSS-NH_2 was grafted onto the HNTs surface.

To evaluate the differences in the surface behavior, the dispersion characteristics of HNTs and HNTs-POSS in different organic solvents are shown in Fig. 3. It is observed that the pristine HNTs

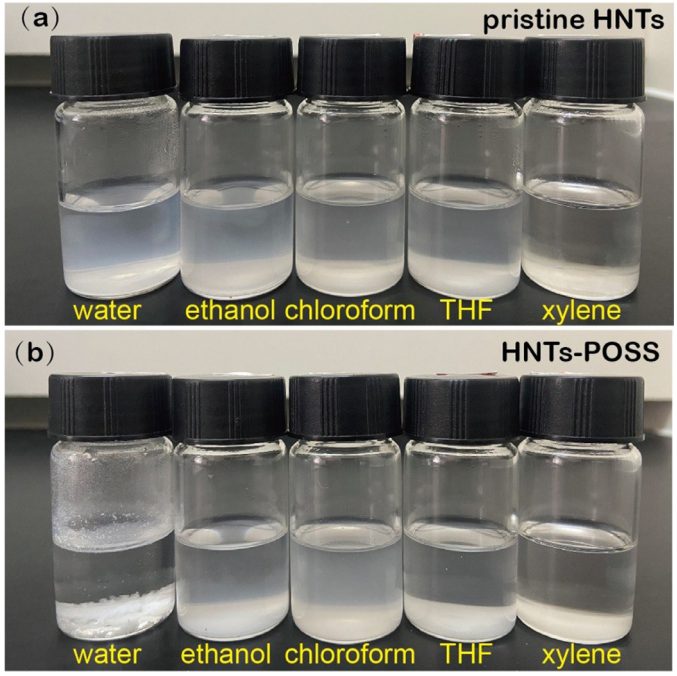

Fig. 3. Digital images of (a) pristine HNTs, and (b) HNTs-POSS dispersed in different solvents (1 mg mL^{-1}. The digital images were taken after 24 h storage).

are well dispersed in water due to the abundance of hydroxyl groups on the surface of HNTs. After the modification, the HNTs-POSS settles at the bottom and the aqueous in the container is clear, indicating HNTs-POSS has a hydrophobic surface. In addition,

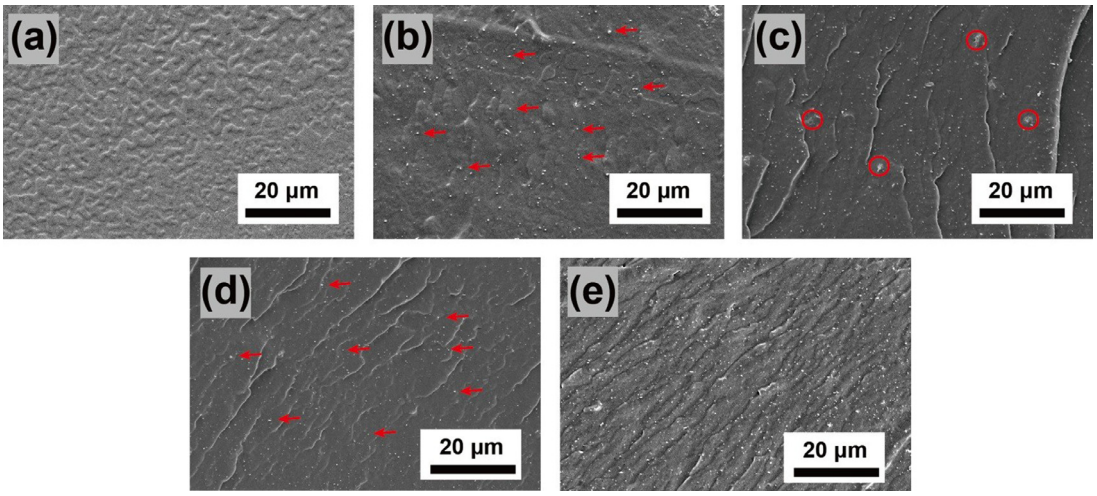

Fig. 4. SEM images of fracture surfaces of pure TPU and its nanocomposites. (a) TPU, (b) HNTs-0.5, (c) HNTs-2, (d) HNTs-POSS-0.5, and (e) HNTs-POSS-2.

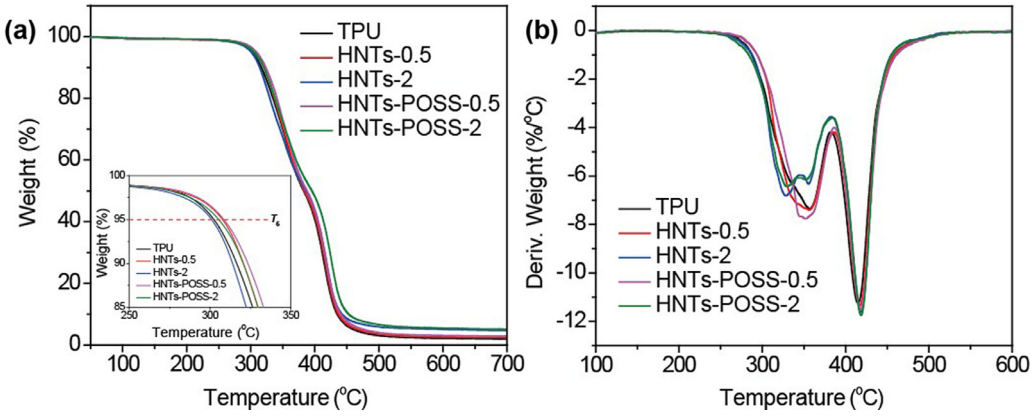

Fig. 5. (a) TGA and (b) DTG curves of TPU and its composites under nitrogen atmosphere.

both of HNTs and HNTs-POSS can be suspended in chloroform to some extent. This phenomenon may be due to the presence of the alkyl chain in the grafted POSS.

3.2. Morphology of fracture surfaces of TPU nanocomposites

To investigate the interfacial interaction between the fillers and polymer matrix, and the dispersion of nano-fillers in TPU matrix, the SEM images of the fracture surfaces of TPU nanocomposites were shown in Fig. 4. The pure TPU in Fig. 4(a) exhibits a typical phase separation structure [30]. As shown in Fig. 4(b, d), it is notable that both pristine HNTs and HNTs-POSS (bright spots in the SEM images marked by red arrows) dispersed uniformly in the TPU matrix at low concentration. In addition, the two-phase structure of TPU gradually disperses with the increasing content of filler in Fig. 4(b–e), indicating these nanofillers destruct the hydrogen bonds of TPU [31]. When the pristine HNTs concentration increased to 2 wt%, some aggregations (red circles) appear in Fig. 4(c). Furthermore, the fracture surfaces of TPU/HNTs-POSS nanocomposites appear to be much rougher than those of TPU/HNTs nanocomposites, suggesting that the incorporation of HNTs-POSS could dissipate more energy during fracture [32].

3.3. Thermal stability of TPU nanocomposites

The thermal stability of TPU nanocomposites was evaluated by TGA, as shown in Fig. 5. The thermal parameters, including temperatures at 5% weight loss (T_5), temperatures at maximum weight loss rate (T_{p1} and T_{p2}), and char yields at 700 °C were listed in Table 2. The thermal decomposition of pure TPU can be divided into two main stages, which is consistent with previous research [5,33]. The first stage occurs in the range of 250–380 °C, which corresponds to the dissociation of the urethane bonds in the TPU hard segments [34]. The second stage between 380–520 °C is due to the thermal decomposition of the soft segments [35]. In comparison with pure TPU, the incorporation of HNTs and HNTs-POSS does not change the apparent degradation pathway in nitrogen except the higher char yield. The increased char yield may result from the incorporation of HNTs means the formation of the effective barrier layer in composites. In addition, the thermal decomposition of POSS contributes to forming a ceramified char made of a polyaromatic silicon structure network [13]. In Fig. 2(a), it is observed that the T_5 values of all TPU nanocomposites except HNTs-2 are higher than that of pure TPU. The TPU/HNTs-POSS nancom-

Table 2
TGA data and LOI values of TPU nanocomposites.

Sample	T_5 (°C)	T_{p1} (°C)	T_{p2} (°C)	Char yields at 700 °C (wt%)	LOI (%)
TPU	302.5	357.1	415.2	1.97	21.7
HNTs-0.5	307.8	351.7	417.3	2.37	22.3
HNTs-2	300.2	352.8	417.6	4.72	24.7
HNTs-POSS-0.5	308.6	356.6	417.0	2.88	24.0
HNTs-POSS-2	304.3	355.8	417.9	5.41	26.3

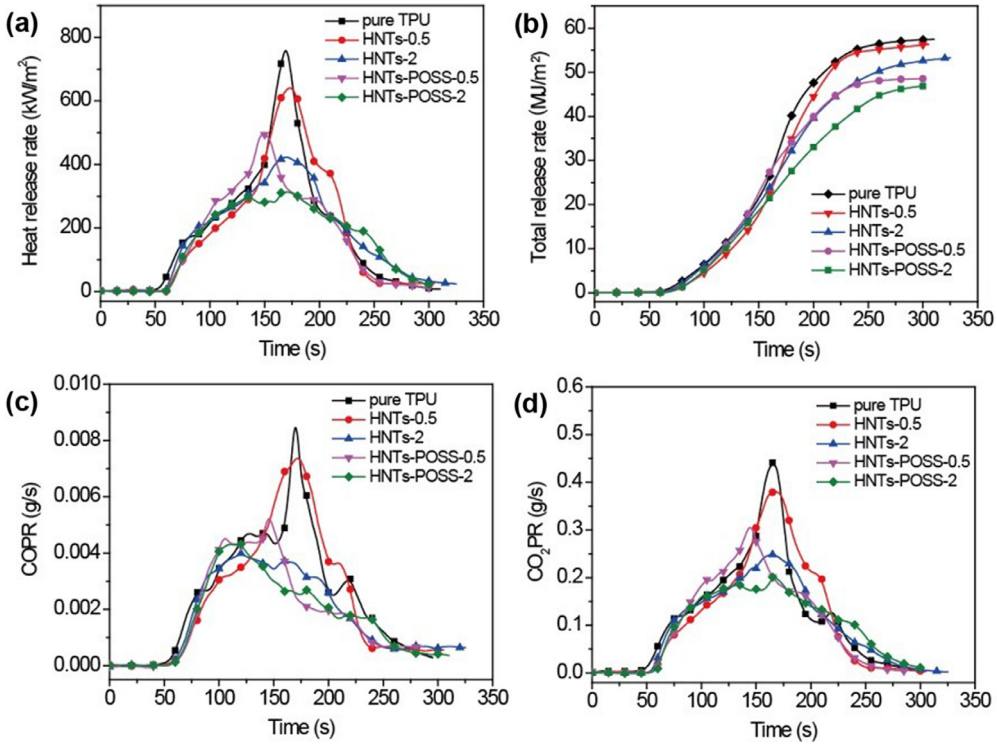

Fig. 6. Cone calorimeter curves of TPU composites: (a) HRR, (b) THR, (c) CO production rate, (d) CO_2 production rate as a function of time.

Table 3
Combustion data of TPU nanocomposites obtained from cone calorimeter measurements at 35 kW/m^2.

Sample	TTI (s)	PHRR (kW/m^2)	THR (MJ/m^2)	PCOPR (g/s)	PCO_2PR (g/s)	Total smoke (m^2/m^2)	Char residues (wt%)
TPU	54±1	788.5±20	57.3±0.4	0.0094±0.0003	0.437±0.010	671.6±20.3	4.2±1.0
HNTs-0.5	62±3	645.3±15	56.2±0.4	0.0073±0.0007	0.383±0.007	622.8±18.5	4.6±1.2
HNTs-2	64±2	426.7±30	53.3±0.7	0.0041±0.0004	0.249±0.013	545.3±30.1	5.7±0.9
HNTs-POSS-0.5	63±3	495.6±24	48.5±0.3	0.0052±0.0004	0.304±0.006	602.2±24.3	5.3±0.8
HNTs-POSS-2	62±1	315.1±35	46.8±0.5	0.0043±0.0005	0.201±0.009	484.7±26.5	8.4±1.0

posites have better thermal stability than those of TPU/HNTs nanocomposites. This phenomenon may be due to the barrier effects of HNTs and HNTs-POSS is more profound than the dehydration of interlayer water in HNTs [36]. The above results indicate that the catalytic charring effect of HNTs-POSS hybrid can enhance the thermal stability of TPU, which is conducive to improving the fire safety of TPU.

3.4. Fire performance of TPU nanocomposites

The burning behavior of TPU nanocomposites was evaluated by limited oxygen index (LOI), as shown in Table 2. The LOI value of pure TPU was 21.7, indicating that TPU was flammable. With the addition of HNTs and HNTs-POSS, the LOI value of TPU nanocomposites wasn't effectively increased. The TPU nanocomposite containing 2 wt% HNTs-POSS achieved a maximum LOI value of 26.3. The slight increase in LOI was ascribed to the low addition of nanofillers, which was similar to other TPU nanocomposites [37,38].

Cone calorimeter is a useful tool to estimate the real fire performance of materials [39]. Fig. 6 shows the time to ignition (TTI), heat release rate (HRR), total heat release (THR), carbon monoxide production rate (COPR) and carbon dioxide production rate (CO_2PR) of TPU nanocomposies as a function of time. The parameters of cone calorimeter tests are summarized in Table 3. It is observed that pure TPU burns violently with a peak value of HRR (PHRR) up to 788.5 kW/m^2 and a THR value of 57.3 MJ/m^2 in Fig. 6(a, b). The obvious suppressions in PHRR and THR of TPU nanocomposites are obtained with the increasing of filler content. Moreover, the HNTs-POSS possess a highly flame retardancy efficient as compared with that of pure HNTs under the same loading. With the addition of 2 wt% HNTs-POSS, the PHRR and THR of TPU nanocomposites are declined to 315.1 kW/m^2 and 46.8 MJ/m^2 with a reduction of 60.0% and 18.3%, respectively. In Table 3, the TTI of TPU nanocomposites is postponed from 54 s to 62 s as compared with pure TPU, indicating the enhancement of thermal stability in a real fire accident. It is ascribed that released crystal water from HNTs as well as the barrier effect of HNTs and POSS postpone the ignition. Interestingly, the TTI of HNTs-POSS-2 is lower than that of HNTs-POSS-0.5. This is due to POSS will decompose earlier than neat TPU resin, as shown in Fig. 2(d), which is consistent with other POSS-based composites [40,41]. Furthermore, the char residue of TPU nanocomposites containing 2 wt% HNTs-POSS is increased from 3.3 wt% for pure TPU to 7.9 wt% after cone calorimeter tests. It indicates that the presence of HNTs-POSS in the TPU matrix contributes to generating sufficient residual char and results in the suppression of heat release effectively. A mass of CO is a big threat during the real fire accident [42]. Fig. 6(c) shows the CO production rate as a function of time. It is noted that the peak production rate of CO (PCOPR) for pure TPU was up to 0.0094 g/s. The incorporation of 2 wt% HNTs-POSS into the TPU matrix results in the maximum reduction in PCOPR (54.3%), which can provide valuable escape time in fire accidents. The total smoke release (TSR) curves in Fig. 6(d) exhibits that the TSR for HNTs-POSS-2 de-

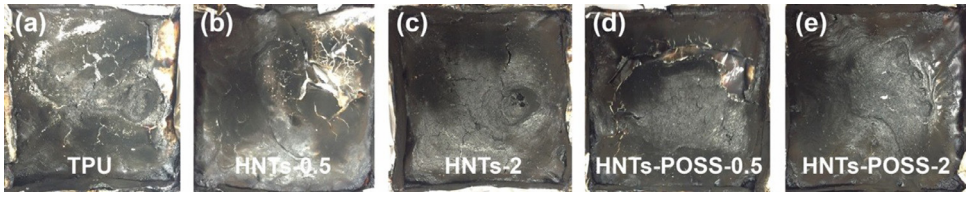

Fig. 7. Digital photos of char residues of (a) pure TPU, (b) HNTs-0.5, (c) HNTs-2, (d) HNTs-POSS-0.5, (e) HNTs-POSS-2; after cone calorimeter test.

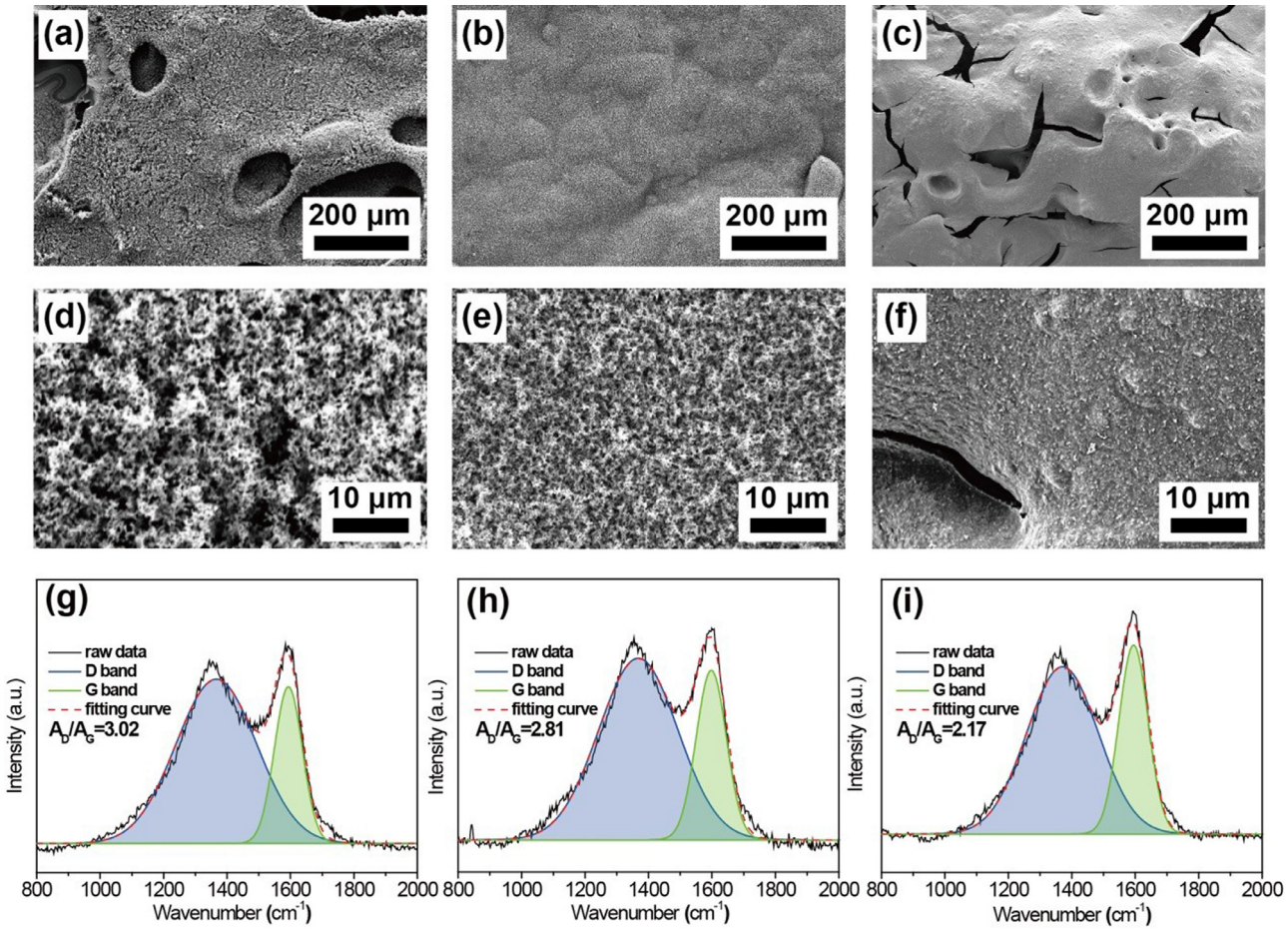

Fig. 8. SEM images of char residues of (a, d) pure TPU, (b, e) HNTs-2, and (c, f) HNTs-POSS-2; Raman spectra of (g) pure TPU, (h) HNTs-2, and (i) HNTs-POSS-2 after cone calorimeter test.

creases to 484.7 m^2/m^2, which is reduced by 27.8% as compared to that of pure TPU. These above results indicate that the addition of HNTs-POSS can serve as flame retardant filler to suppress the heat release, PCO_2PR, PCO_2PR and TSR of TPU nanocomposite effectively during fire accidents.

3.5. Analysis of condensed phase

The morphologies and graphitization degree of the residual chars were presented in Figs. 7 and 8 to analyze the condensed phase. The digital images in Fig. 7 reveal that the char residues are increased with the increasing content of HNTs or HNTs-POSS. As shown in Fig. 8(a) and (d), the char residue of pure TPU has a fragile and loose structure with big holes, which would provide a considerable path for the volatile gaseous to escape. With the addition of HNTs, the char residue of HNTs-2 (Fig. 8(b) and (e)) obtains more continuous structure with smaller pores, which will inhibit the volatile gaseous from evaporating as compared to that of pure TPU. On the contrary, HNTs-POSS-2 in Fig. 8(c) and (f) exhibits more compact and integrated char layers. It is ascribed to the thermal decomposition of POSS can form a ceramified silicon char network in a polyaromatic structure [13]. The continuous char residue could prevent the heat transfer and suppress smoke generation of TPU during combustion, thus improving the fire safety of TPU. In addition, it is clearly observed that many HNTs disperse on the surface of char residue in Fig. 8(f). Raman spectra were utilized to determine the graphitization degree of char residues, as shown in Fig. 8(g–i). There are two fitted peaks located at around 1362 and 1594 cm^{-1}, which correspond to D band and G band, respectively. The fitted area ratio (A_D/A_G) represents the degree of graphitization [43]. It is noteworthy that the values for A_D/A_G of pure TPU, HNTs-2 and HNTs-POSS-2 are 3.02, 2.87 and 2.17, respectively. The lower value of A_D/A_G means the formation of a higher graphitization degree. The result implies that the addition of HNTs-POSS facilitates to forming more graphitized char residue with the shield effect for underlying polymer. Thus, the combustion of the underlying polymer can be inhibited more effectively by hindering the transfer of heat and volatile gaseous [44].

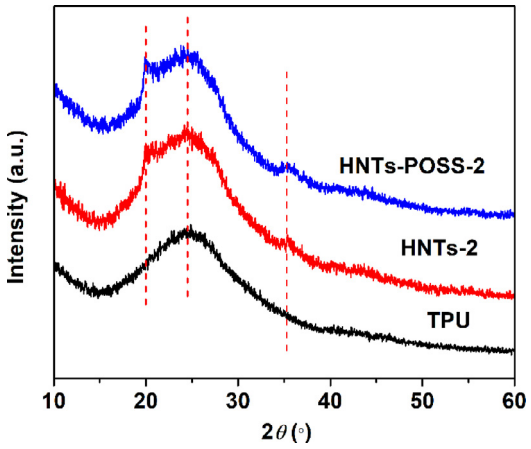

Fig. 9. XRD patterns of the char residues for pure TPU, HNTs-2, and HNTs-POSS-2.

The XRD patterns of the char residues are shown in Fig. 9. A strong and board peak observed at 24.9° in pure TPU is assigned to the (002) lattice planes of graphite, reflecting the generation of graphitized carbon [45]. With the addition of HNTs or HNTs-POSS, the width of the characteristic peak at 24.9° becomes narrow, indicating an increase in near-graphitization. In addition, two weak peaks appearing at 2θ angles of 20.1° and 35.3° in HNTs-2 and HNTs-POSS-2 were attributed to the lattice planes for HNTs [25,46].

3.6. Analysis of evolved gases

In order to simulate and monitor the release of volatile products during the thermal decomposition process [47], the TG-IR results of pure TPU, HNTs-2 and HNTs-POSS-2 are shown in Fig. 10. The three-dimensional (3D) TG-IR spectra shown in Fig. 10(a–c) demonstrate that the incorporation of HNTs-POSS can inhibit the release of volatile gaseous. It is observed that the intensity of volatile products of HNTs-POSS-2 is much lower than that of HNTs-2, indicating HNTs-POSS has a better suppression effect on the pyrolysis products than pristine HNTs. The Gram-Schmidt curves in Fig. 10(d) reveals the total absorbance intensity of the pyrolysis products. It is clear that the total absorbance intensity of pyrolysis products for HNTs-POSS-2 is the weakest among the three samples, suggesting that HNTs-POSS-2 released the least amount of gas during thermal decomposition. The decomposed products at maximum mass loss rate of three samples in Fig. 10(e) show similar characteristic peaks. The major products of pure TPU and

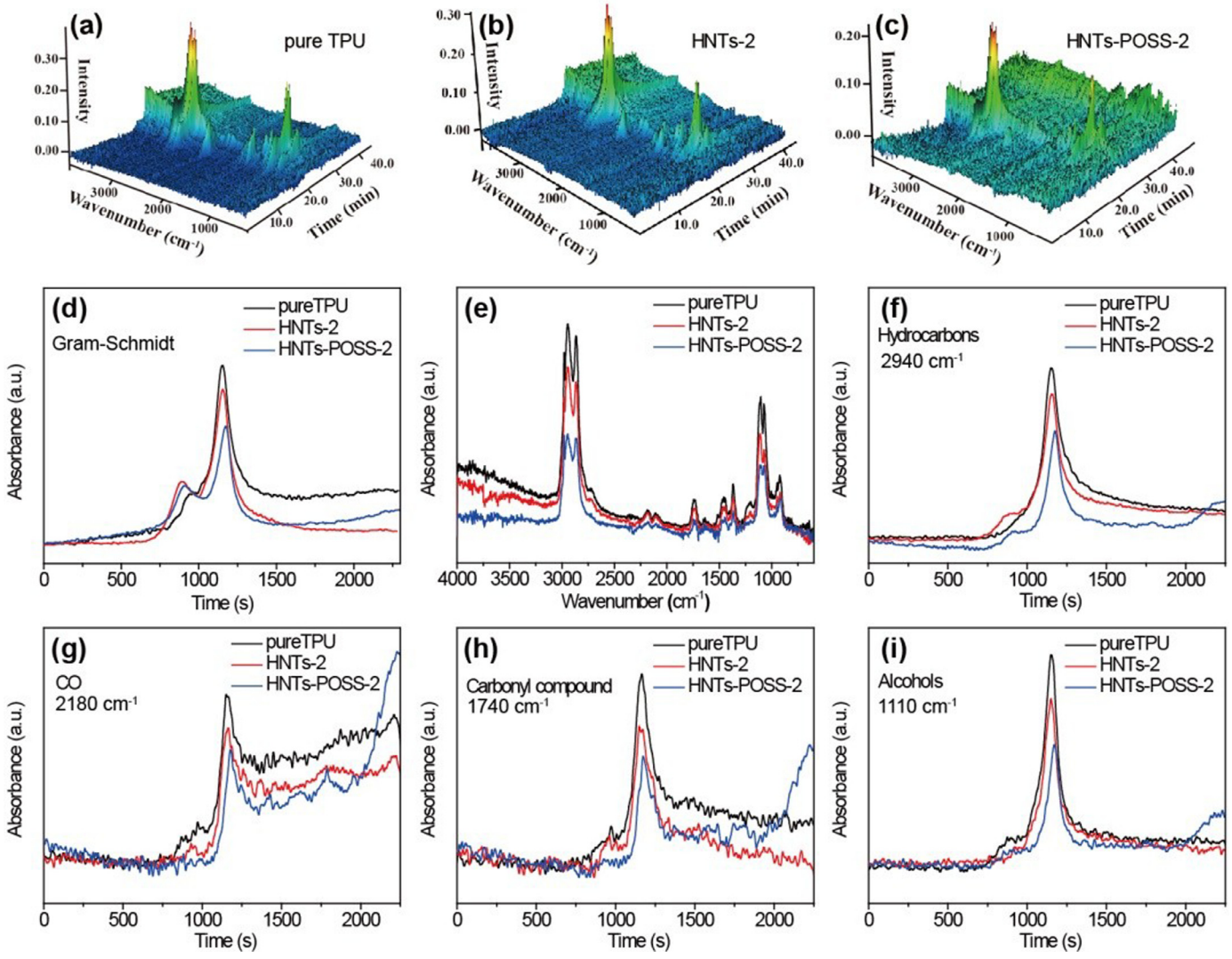

Fig. 10. 3D TG-FTIR spectra of (a) TPU, (b) HNTs-2, and (c) HNTs-POSS-2. Absorbance of pyrolysis products for TPU, HNTs-2, and HNTs-POSS-2 as a function of time: (d) Gram-Schmidt, (e) at maximum mass loss rate, (f) CO, (g) hydrocarbons, (h) carbonyl compounds, and (i) alcohols.

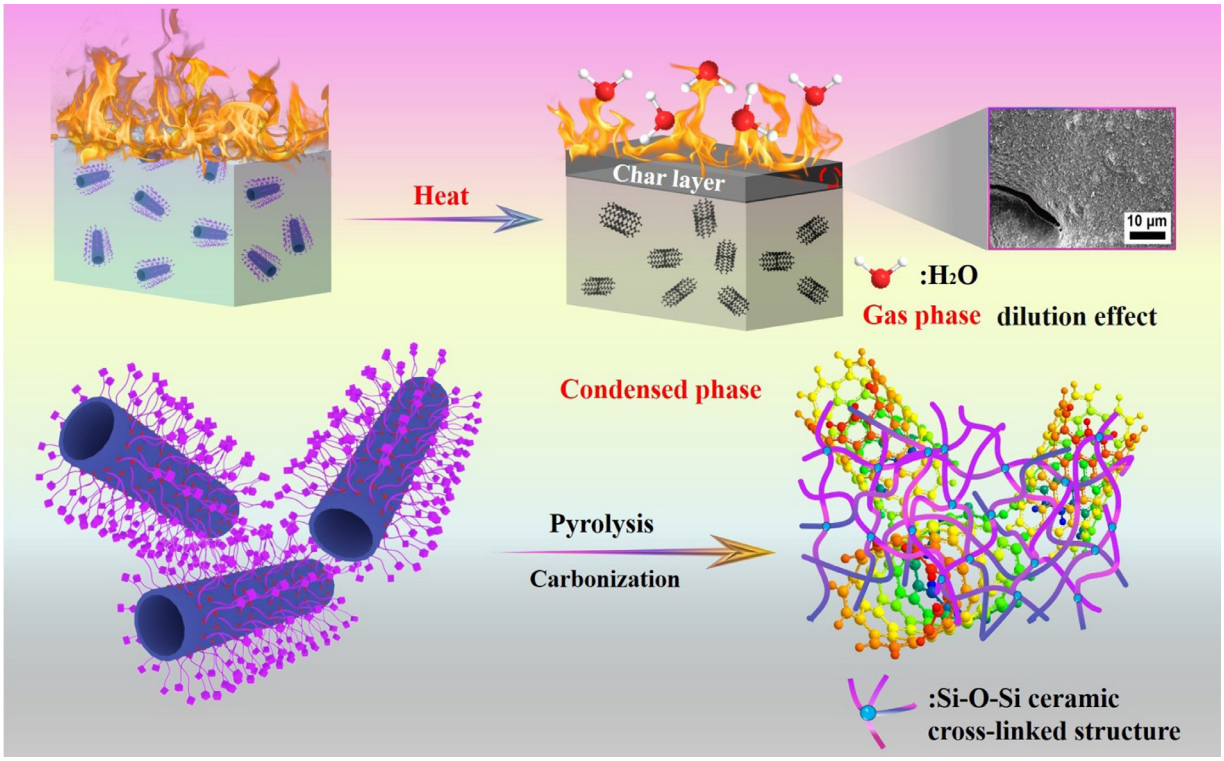

Fig. 11. Schematic diagram of flame retardant mechanism of TPU/HNTs-POSS composites.

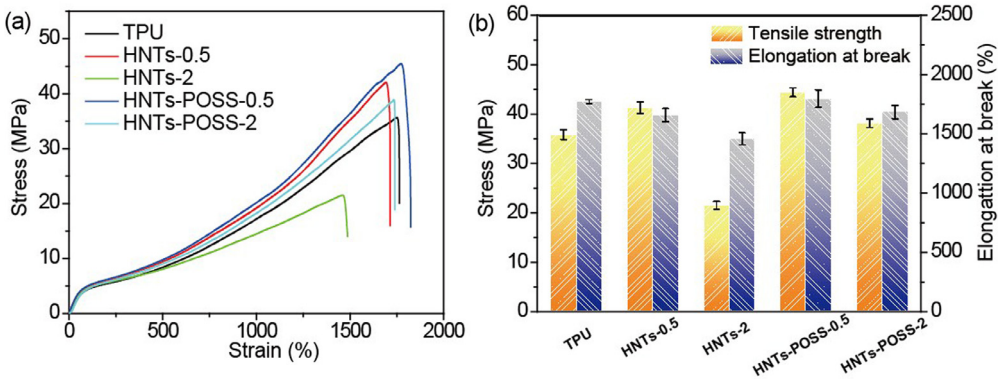

Fig. 12. (a) Stress versus strain curves, and (b) tensile properties of TPU and its composites.

its nanocomposites, including hydrocarbons (2940 cm^{-1}), CO (2180 cm^{-1}), carbonyl compound (1740 cm^{-1}), and alcohols (1110 cm^{-1}) are presented in Fig. 10(f–i), respectively [48]. Similarly, the signal intensity of various gaseous from HNTs-POSS-2 is significantly lower than that of pure TPU. The above results demonstrated that the introduction of HNTs-POSS can effectively suppress the release of gaseous degradation products, which can be attributed to the continuous and compact char barrier network that can block the mass transfer of decomposed volatiles.

3.7. Flame retardant mechanism

Based on the mentioned analysis above, the possible flame retardant mechanism of TPU/HNTs-POSS nanocomposite was speculated and illustrated in Fig. 11. Bourbigot et al. demonstrated that the thermal decomposition of POSS/TPU composites will form a Si-O-Si spatial network in a polyaromatic structure during combustion [13]. In addition, it is observed that many HNTs are immersed in the compact char layer, as revealed by Fig. 8(f). The integrated and dense char residues, consisting of HNTs, ceramified silicon network and carbonaceous layers, could serve as an effective protective shield for the underlying polymer matrix and slow down flame propagation and spread, thus improving the fire safety of TPU [49]. On the other hand, the loss of crystal water from HNTs can dilute the combustible volatiles and then decline the combustion intensity to some extent. Thus, the release of heat and smoke of TPU nanocomposites were dramatically restrained.

3.8. Mechanical property of TPU composites

The mechanical properties of TPU composites were investigated by tensile tests. The tensile stress-strain curves and the corresponding data are represented in Fig. 12. The tensile strength and elongation at break of pure TPU is 35.9 MPa and 1775.2%, respectively. With the addition of 0.5 wt% of HNTs, the tensile strength of the TPU composite is enhanced to 41.4 MPa, while the elongation at break decreases to 1662.5%. These changes can be attributed to the reinforcement effect of the pristine HNTs is more profound

than the destruction of of hydrogen bonds for TPU at low concentration [23,50,51]. When the content of pristine HNTs increases up to 2 wt%, the higher content of HNTs will bring in more destruction of hydrogen bonds for TPU, resulting in the sharply decrease in the tensile strength and elongation at break of HNTs-2 [37]. In addition, the aggregation of HNTs, as revealed by the SEM images in Fig. 4, will deteriorate the mechanical properties of TPU to some extent. As for HNTs-POSS, the presence of POSS can serve as physical cross-linking points to absorb more energy under external stress [12]. In comparison to HNTs-2, the TPU composites containing 2 wt% HNTs-POSS still exhibited an enhancement in tensile stress (38.2 MPa). Meanwhile, the elongation at break of HNTs-POSS-2 was decreased by 4.9%, much lower than that of pristine HNTs [52]. This is because the POSS functional groups replaced the hydroxyl groups on the surface of HNTs, which reduced the adverse effects of pristine HNTs. Moreover, the presence of bulk POSS introduces strong steric effects that impede the movement of TPU chains, resulting in more efficient load transfer.

4. Conclusions

In this work, POSS was decorated onto the surface of HNTs (HNTs-POSS) by using a silane agent (KH-560) as the chemical bridge. Then HNTs-POSS was mixed with TPU by melt compounding. The SEM observation revealed that HNTs-POSS dispersed homogeneously in TPU matrix due to the presence of POSS prevented the re-aggregation. With the addition of 2.0 wt% HNTs-POSS, the peak of heat release rate (PHRR) and total heat release (THR) of TPU nanocomposite were remarkably decreased by 60.0% and 18.3%, respectively. Moreover, the HNTs-POSS-2 also exhibited an obvious reduction in the peak CO production rate (54.3%), the peak CO_2 production rate (54.0%) and total smoke release (27.8%). The Si-O-Si spatial network from the decomposition of POSS in combination with the HNTs and the char residue from TPU matrix formed a continuous and compact char layer, which was responsible for the enhanced fire safety and smoke suppression of TPU/HNTs-POSS nanocomposite. In addition, the tensile tests exhibited that the addition of 2 wt% HNTs-POSS did not sacrifice the ductility of TPU nanocomposites. This work demonstrates a feasible method for improving the fire safety of TPU, potentially broadening the potential applications of TPU nanocomposites.

Declaration of Competing Interest

The authors declare that they have no known competing financial interests or personal relationships that could have appeared to influence the work reported in this paper.

Acknowledgments

This work was financially supported by the National Key Research and Development Program of China (No. 2016YFB0302300), the International Collaboration Programs of Guangdong Province (No. 2020A0505100010), the Fundamental Research Funds for the Central Universities (No. 2019MS062), the Natural Science Foundation of Guangdong Province (No. 2021A1515012425), the Overseas Famous Scholar Funds of Guangdong Province (No. 2020A1414010372), City University of Hong Kong (No. 9678103), and the Opening Project of Key Laboratory of Polymer Processing Engineering (South China University of Technology), Ministry of Education of China (No. KFKT1904).

References

[1] S.M. Kim, H. Jeon, S.H. Shin, S.A. Park, J. Jegal, S.Y. Hwang, D.X. Oh, J. Park, Adv. Mater. 30 (2018) 1705145.
[2] T. Vijayakanth, F. Ram, B. Praveenkumar, K. Shanmuganathan, R. Boomishankar, Chem. Mater. 31 (2019) 5964–5972.
[3] L.X. He, J.L. Wang, B.B. Wang, X. Wang, X. Zhou, W. Cai, X.W. Mu, Y.B. Hou, Y. Hu, L. Song, Compos. Part B Eng. 179 (2019) 107486.
[4] W.Q. Lei, C.Q. Fang, X. Zhou, J.B. Li, R. Yang, Z.S. Zhang, D.H. Liu, J. Mater. Sci. Technol. 33 (2017) 1424–1432.
[5] C. Liu, W. Wu, Y.Q. Shi, F.Q. Yang, M.H. Liu, Z.X. Chen, B. Yu, Y.Z. Feng, Compos. Part B Eng. 203 (2020) 108486.
[6] Y.Q. Shi, B. Yu, K.Q. Zhou, R.K.K. Yuen, Z. Gui, Y. Hu, S.H. Jiang, J. Hazard. Mater. 293 (2015) 87–96.
[7] X.Y. Ji, D.Y. Chen, Q.W. Wang, J.B. Shen, S.Y. Guo, Compos. Sci. Technol. 163 (2018) 49–55.
[8] H. Chen, C. Deng, Z.Y. Zhao, S.C. Huang, Y.X. Wei, Y.Z. Wang, Compos. Part B Eng. 199 (2020) 108315.
[9] W.Z. Xu, C.M. Cheng, Z.Q. Qin, D. Zhong, Z.H. Cheng, Q.Q. Zhang, Polym. Adv. Technol. 32 (2021) 228–240.
[10] B. Yu, B. Tawiah, L.Q. Wang, A.C.Y. Yuen, Z.C. Zhang, L.L. Shen, B. Lin, B. Fei, W. Yang, A. Li, S.E. Zhu, E.Z. Hu, H.D. Lu, G.H. Yeoh, J. Hazard. Mater. 374 (2019) 110–119.
[11] L. Tang, J. Dang, M.K. He, J.Y. Li, J. Kong, Y.S. Tang, J.W. Gu, Compos. Sci. Technol. 169 (2019) 120–126.
[12] H. Zhao, W. She, D. Shi, W. Wu, Q.C. Zhang, R.K.Y. Li, Compos. Part B Eng. 177 (2019) 107441.
[13] S. Bourbigot, T. Turf, S. Bellayer, S. Duquesne, Polym. Degrad. Stabil. 94 (2009) 1230–1237.
[14] S. Spoljaric, R.A. Shanks, J. Appl. Polym. Sci. 126 (2012) E440–E454.
[15] W. Guo, W. Liu, L. Xu, P. Feng, Y.R. Zhang, W.J. Yang, C.J. Shuai, J. Mater. Sci.Technol. 46 (2020) 237–247.
[16] W. Wu, X.W. Cao, H. Lin, G.J. He, M.M. Wang, J. Polym. Res. 22 (2015) 177.
[17] W. Wu, X.W. Cao, Y.J. Zhang, G.J. He, J. Appl. Polym. Sci. 130 (2013) 443–452.
[18] M. Wu, W. Liu, J.R. Yao, Z.Z. Shao, X. Chen, J. Mater. Sci.Technol. 63 (2021) 203–209.
[19] L. Zhou, Y. He, H. Shi, G.Q. Xiao, S.H. Wang, Z.Y. Li, J.Y. Chen, J. Hazard. Mater. 380 (2019) 120865.
[20] R.J. Smith, K.M. Holder, S. Ruiz, W. Hahn, Y.X. Song, Y.M. Lvov, J.C. Grunlan, Adv. Funct. Mater. 28 (2018) 1703289.
[21] M. Rajaei, N.K. Kim, S. Bickerton, D. Bhattacharyya, Compos. Part B Eng. 165 (2019) 65–74.
[22] E. Jasinski, V. Bounor-Legare, A. Taguet, E. Beyou, Polym. Degrad. Stabil. 183 (2021) 109407.
[23] E.S. Goda, K.R. Yoon, S.H. El-sayed, S.E. Hong, Thermochim. Acta 669 (2018) 173–184.
[24] M. Sahnoune, A. Taguet, B. Otazaghine, M. Kaci, J.M. Lopez-Cuesta, Polym. Eng. Sci. 59 (2019) 526–534.
[25] S. Shang, X. Ma, B.H. Yuan, G.Q. Chen, Y.R. Sun, C.Y. Huang, S. He, H.M. Dai, X.F. Chen, Compos. Part B Eng. 177 (2019) 107371.
[26] Y.H. Wang, C. Liu, J.J. Lai, C.L. Lu, XM Wu, Y.Q. Cai, L.Q. Gu, L.T. Yang, G.H. Zhang, G. Shi, Polym. Test. 81 (2020) 106174.
[27] S.H. Wang, J.S. Li, W.J. Wang, X.G. Wang, H.F. Li, J. Sun, B. Fei, X.Y. Gu, S. Zhang, Compos. Part A Appl. Sci. Manuf. 140 (2021) 106170.
[28] X.B. Jin, E. Xiang, R. Zhan, D.C. Qin, M.L. Jiang, Z.H. Jiang, J. Appl. Polym. Sci. 138 (2021) e49621.
[29] W. Wu, X.W. Cao, J. Luo, G.J. He, Y.J. Zhang, Polym. Compos. 35 (2014) 847–855.
[30] D. Pedrazzoli, I. Manas-Zloczower, Polymer 90 (2016) 256–263.
[31] E. Ayandele, B. Sarkar, P. Alexandridis, Nanomater. Basel 2 (2012) 445–475.
[32] X.L. Li, X.X. Sheng, Y.Q. Guo, X. Lu, H. Wu, Y. Chen, L. Zhang, J.W. Gu, J. Mater. Sci. Technol. 86 (2021) 171–179.
[33] Y.Q. Shi, C. Liu, Z.P. Duan, B. Yu, M.H. Liu, P.A. Song, Chem. Eng. J. 399 (2020) 125829.
[34] D. Tabuani, F. Bellucci, A. Terenzi, G. Camino, Polym. Degrad. Stabil. 97 (2012) 2594–2601.
[35] W. Cai, X.W. Mu, Y. Pan, W.W. Guo, J.L. Wang, B.H. Yuan, X.M. Feng, Q.L. Tai, Y. Hu, Polym. Adv. Technol. 29 (2018) 2545–2552.
[36] L.J. Chen, Z.X. Jia, X.H. Guo, B.C. Zhong, Y.J. Chen, Y.F. Luo, D.M. Jia, Chem. Eng. J. 336 (2018) 748–756.
[37] L.B. Liu, Y. Xu, S. Li, M.J. Xu, Y.T. He, Z.X. Shi, B. Li, Compos. Part B Eng. 176 (2019) 107218.
[38] J.L. Wang, D.C. Zhang, Y. Zhang, W. Cai, C.X. Yao, Y. Hu, W.Z. Hu, J. Hazard. Mater. 362 (2019) 482–494.
[39] X.W. Cao, X.N. Chi, X.Q. Deng, Q.J. Sun, X.J. Gong, B. Yu, A.C.Y. Yuen, W. Wu, R.K.Y. Li, Polym. Basel 12 (2020) 1105.
[40] S.D. Jiang, G. Tang, Z.M. Bai, Y.Y. Wang, Y. Hu, L. Song, RSC Adv. 4 (2014) 3253–3262.
[41] X. Wang, Y. Hu, L. Song, H. Yang, B. Yu, B. Kandola, D. Deli, Thermochim. Acta 543 (2012) 156–164.
[42] W. Wu, H.B. He, T. Liu, R.C. Wei, X.W. Cao, Q.J. Sun, S. Venkatesh, R.K.K. Yuen, V.A.L. Roy, R.K.Y. Li, Compos. Sci. Technol. 168 (2018) 246–254.
[43] X.W. Cao, X.N. Chi, X.Q. Deng, T. Liu, B. Yu, B. Wang, A.C.Y. Yuen, W. Wu, R.K.Y. Li, Polym. Adv. Technol. 31 (2020) 1661–1670.
[44] H.W. Wang, H. Qiao, J. Guo, J. Sun, H.F. Li, S. Zhang, X.Y. Gu, Compos. Part B Eng. 182 (2020) 107498.
[45] L.W. Yan, H. Zhang, S.T. Zhou, H.W. Zou, Y. Chen, M. Liang, J. Appl. Polym. Sci. 138 (2021) e50030.
[46] M.L. Du, B.C. Guo, D.M. Jia, Eur. Polym. J. 42 (2006) 1362–1369.
[47] X.L. Chen, W.D. Wang, C.M. Jiao, J. Hazard. Mater. 331 (2017) 257–264.

[48] W. Cai, B.B. Wang, L.X. Liu, X. Zhou, F.K. Chu, J. Zhan, Y. Hu, Y.C. Kan, X. Wang, Compos. Part B Eng. 178 (2019) 107462.
[49] W.J. Zhang, G. Camino, R.J. Yang, Prog. Polym. Sci. 67 (2017) 77–125.
[50] L. Tang L, J.L. Zhang, J.W. Gu, Chinese J. Aeronaut. 34 (2021) 659–668.
[51] J. Zhao, J.L. Zhang, L. Wang, J.K. Li, T. Feng, J.C. Fan, L.X. Chen, J.W. Gu, Compos. Commun. 22 (2020) 100486.
[52] W. Cai, Y.X. Hu, Y. Pan, X. Zhou, F.K. Chu, L.F. Han, X.W. Mu, Z.Y. Zhuang, X. Wang, W.Y. Xing, J. Colloid Interface Sci. 561 (2020) 32–45.